

Investigation of New Sectored Hemispherical Dielectric Resonator Antennas Operating at TM_{101} and TE_{111} Mode for Circular Polarization

Rakesh Chowdhury and Raghvendra Kumar Chaudhary*

Abstract—This article discusses the effect of sectorization technique in a hemispherical dielectric resonator antenna (HDRA) for the first time with its significant effects on electromagnetic modes and various antenna parameters. The sector angle (β) forms an additional framework for better optimization of HDRA. The resonance frequency, impedance bandwidth, co-cross polarization characteristics have been investigated in new sectored HDRA geometries excited at their TE_{111} and TM_{101} modes. Further, examination of circular polarization (CP) is carried out by detuning of degenerate orthogonal modes in HDRAs, and $\beta = 180^\circ$ has been particularly examined in details for CP. Based on the results, appropriate values of ' β ' and probe position (P_r) are chosen followed by modelling a prototype and experimental.

1. INTRODUCTION

Over the past few decades, dielectric resonator antennas (DRAs) have been given noteworthy research effort by scientific community around the globe for different antenna applications. It offers good radiation efficiency, wide impedance bandwidth, several modes with unique radiation pattern, and high design flexibility [1]. Most popular shapes are cylindrical and rectangular DRAs whereas hemispherical shaped DRAs are least used due to absence of any design flexibility in choosing the geometrical parameter as HDRAs have zero degree of freedom [2]. Early research on HDRAs was based on numerical studies for calculation of resonance frequency/quality factor, input impedance, and radiation pattern [3, 4]. Thus, this area is not fully explored for various applications. However, several techniques have been reported in literature to improve the performance of HDRAs by tailoring its conventional shape. For example, a two-layer non-homogeneous HDRA was reported in [5], and maximum 31.9% impedance bandwidth was achieved. However, this technique increased the system complexity and was not feasible for practical applications. Also, an impedance bandwidth of 83% was achieved in [6] using conventional HDRA in an inverted arrangement, but stability of this structure is not preferable for practical use. Recently, a more feasible modification was presented by Guha and Antar using a half-split DRA [7] and segmented HDRAs [8] for wide-band applications. However, these geometries used multi-segmented DRAs and did not incorporate the investigation of sector angle. Hence, the background on sectored HDRA is not explored and is the motivation of this work. From the investigation of sectorization technique, it has been found that sectored HDRAs also support circular polarization [CP] as a result from detuning of degenerate modes. This study is very important because there are few researches available in literature that claim CP in HDRA geometries [9, 10]. Thus, in the past people focused on only one form of DRA in which the sectorization effects were not included, and the performed analysis was

Received 16 April 2020, Accepted 24 June 2020, Scheduled 9 July 2020

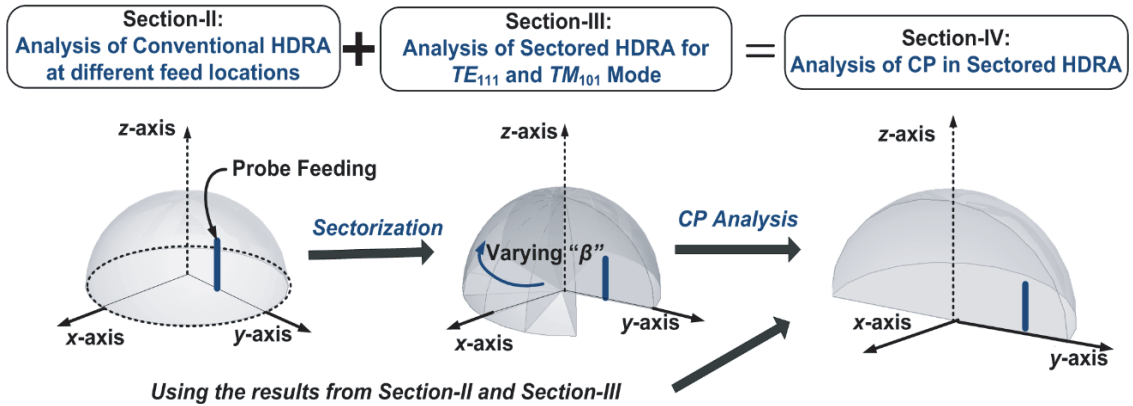
* Corresponding author: Raghvendra Kumar Chaudhary (raghvendra.chaudhary@gmail.com).

The authors are with the Department of Electronics Engineering, Indian Institute of Technology (Indian School of Mines), Dhanbad, Jharkhand 826004, India.

Table 1. Comparison among reported modifications in conventional hemispherical DRAs.

Ref.	Available Approaches in literature, (ϵ_r , Feature)	β	Measured Bandwidth (BW) %		Ground Plane size
			Impedance BW	Axial ratio BW	
[7]	Using Multi-Element Approach, (10, two elements)	180°	35% (2.9–3.88 GHz)	Nil	90 × 90 mm ²
[8]	Using Multi-Element Approach, (10, four elements)	90°	26% (2.7–3.5 GHz)	Nil	90 mm Diameter
[5]	Using Multi-Layer Approach, (6.85, 2.5, complex)	360°	31.9% (2.87–3.96 GHz)	Nil	60 mm Diameter
[6]	Inverted Geometry Approach, (9.2, Unstable)	360°	83% (1.8–3.7 GHz)	Nil	100 × 100 mm ²
[9]	Using Parasitic Element Approach, (9.5, Low Performance)	360°	22% (3.4–4.83 GHz)	3.4% (3.45–3.57 GHz)	Not Given
This Work	Sectorization Approach, (9.8, simple, stable, single element)	90° to 360°	47.4% (4.28–6.94 GHz)	8.0% (5.13–5.56 GHz)	50 × 50 mm ²

limited to linear polarization only. The idea of sectorization is not new and has been applied on circular cylindrical DRAs [11, 12]. Since HDRA is also a body of revolution, sectorization technique can be used for improving antenna performance. The proposed idea of altering the conventional HDRAs is simple and more feasible for practical use over existing techniques as illustrated in Table-1. From observation, the proposed technique may be more convenient to apply for obtaining better antenna performance and CP designing. The present investigation is characterized by simulation and experimental studies. The chronology of this research article is clarified in Fig. 1. In Section 2, initially a conventional HDRA (without modification) is characterized at different feed locations for exciting TE_{111} and TM_{101} modes. Then, in Section 3, sectorization method is applied, and identification of excited modes are carried out followed by inspecting the effect of sectorization on antenna parameters. Further, CP analysis is performed in Section 4 followed by the prototyping of final design and validations.

**Figure 1.** Chronology and investigation approach adopted in this research work.

2. ANALYSIS OF CONVENTIONAL HEMISPHERICAL DRAS

The design starts with a conventional HDRA as a reference antenna ($r = 11$ mm and $\epsilon_r = 9.8$), excited by a coaxial probe placed over an FR4 glass epoxy grounded substrate as shown in Fig. 2. Before applying sectorization approach, the analysis of conventional HDRA is important to identify the nature

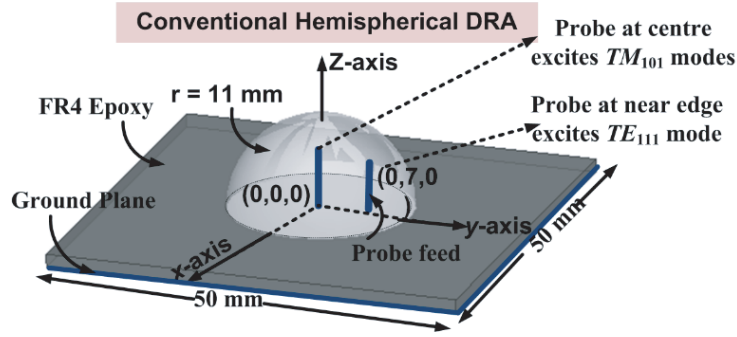


Figure 2. Geometry of conventional HDRA (reference antenna) excited with probe feeding at different locations along y -axis.

of fundamental modes without modification and the position within conventional HDRA where the best coupling can be achieved for excitation of a particular mode. This analysis of conventional HDRA is not presented before, and therefore, $\beta = 360^\circ$ is investigated in this section. A conventional HDRA is formed when $\beta = 360^\circ$ and has been well explored in literature theoretically for fundamental modes TE_{111} (broadside) and TM_{101} (end-fire) [3]. Unlike cylindrical and rectangular DRAs, closed form expression exists for HDRA due to its simple interface, and for field formulation, the z -directed probe current is resolved into r -directed and θ -directed probe currents as in Equation (1) [4].

$$\begin{aligned}
 J_z(\vec{r}')\hat{z} &= J_r(\vec{r}')\hat{r} + J_\theta(\vec{r}')\hat{\theta} \\
 J_r(\vec{r}') &= J_z(\vec{r}')\cos\theta' \\
 J_\theta(\vec{r}') &= -J_z(\vec{r}')\sin\theta'
 \end{aligned}
 \tag{1}$$

where r' refers to the source point, J_r the r -directed current, J_θ the θ -directed current. When probe feed is placed at the center, probe current is more dominated by J_r component as the component of J_θ is zero in this case. As a result, only TM mode is excited in HDRA, but when probe is displaced slightly from the center along y -direction, the component of J_θ also appears along with J_r and excites both TM and TE modes in the structure. Fig. 3 shows $|S_{11}|$ for a conventional HDRA with varying probe feed location along y -axis. It is observed that at the center ($P_r = 0$ mm), only TM_{101} is excited. When the feed is displaced along y -axis away from the center, θ -directed current causes TE modes to appear. For $0 < P_r \leq 3$ mm, only TM_{101} is excited, but after $P_r > 3$, higher order mode TE_{221} is also excited weakly adjacent to TM_{101} and influences its field configuration. Hence, it is not appropriate to consider it as pure TM_{101} , and therefore, both modes are collectively termed as combined mode (in

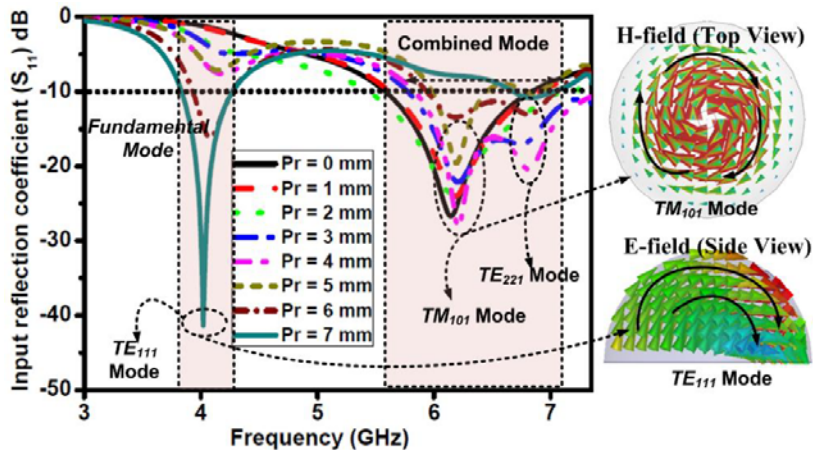


Figure 3. Simulated $|S_{11}|$ of conventional HDRA at different probe locations.

probe position between 4 to 6 mm) in this work. When feed is displaced farther from center, coupling of combined modes decreases, and, at $P_r = 7$, fundamental TE_{111} mode is properly excited in HDRA. So, by choosing proper feed location perfect TE and TM modes are coupled to HDRA, and their electric field distribution is also incorporated in Fig. 3. Unlike cylindrical DRA, the probe feed cannot be placed at the outer circumference in HDRA. The position of feed must be optimized to get the proper location where pure TE and TM modes can be excited which is accomplished in this section. Therefore, it is important to identify the feed position first to excite the fundamental modes on which the rest of analysis depends on that presented in Section 3 and Section 4.

Using the results of Fig. 3, two feed locations are identified which excite perfect TM and TE modes. The approach adopted is to fix the feed at the center ($P_r = 0$ mm) for the first case and vary ' β ' to get different sector geometries thereby observing the effect of sectorization on antenna performance operating at end-fire TM_{101} mode. The same procedure is followed in the second case by keeping the feed at $P_r = 7$ mm for observing the effect of antenna performance operating at broadside TE_{111} mode. Probe height is an important consideration for designing HDRAs; therefore, for each analysis performed in this work, parametric analysis of probe height is carried out, and optimized value is chosen where the best coupling is achieved. Thus, the analysis of probe height is not shown for brevity of this paper. The diameter of probe is small (~ 0.12 cm), and its effects are insignificant in the present design because probe diameter is small as compared to the operating wavelength of the antenna (~ 5.4 cm at center frequency) as well as the probe length which is more than 7 mm above the ground plane.

3. ANALYSIS OF SECTORIZATION EFFECT IN HEMISPHERICAL DRA

The new geometry of non-conventional HDRA formed after sectorization (having radius " r ") is shown in Fig. 4. A spherical wedge-shaped volume has been removed repeatedly from a reference conventional HDRA (shown in Fig. 2) to obtain different sectored geometries formed by setting $90^\circ \leq \beta < 360^\circ$, and to the best of author's knowledge, this technique of sectorization has not been investigated in literature. However, the main focus is given to $\beta = 180^\circ$ in this manuscript where the best CP performance is achieved after performing the analysis of modes in different sectored HDRAs in this section. The new variable design parameter obtained is sector angle symbolized by ' β ' in this paper. Using the results of the previous section, two feed locations are identified ($P_r = 0$ mm and 7 mm) which excites perfect TM and TE modes. Now, the approach adopted is to fix the feed at the center ($P_r = 0$ mm) for the first case and vary ' β ' to get different sector geometries thereby observing the effect of sectorization on antenna performance operating at end-fire TM_{101} mode. In the second case, the same procedure is

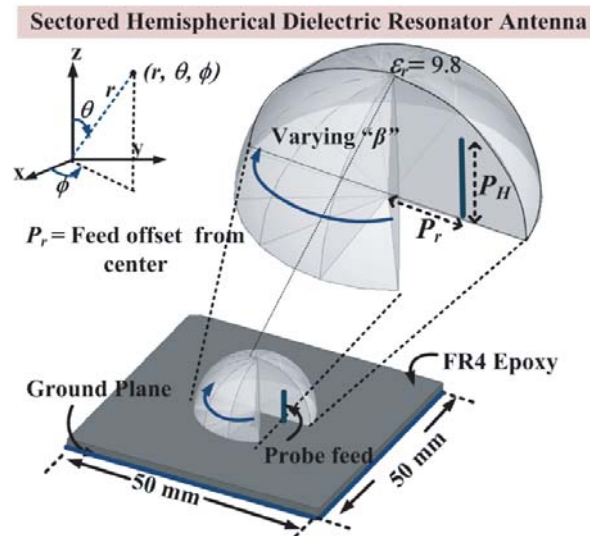


Figure 4. General geometry of sectored hemispherical DRA. Sector angle is varied from $\beta = 360^\circ$ to 90° with step size of 30° . (Final geometry investigated is $\beta = 180^\circ$ at Probe position $P_r = 6$ mm).

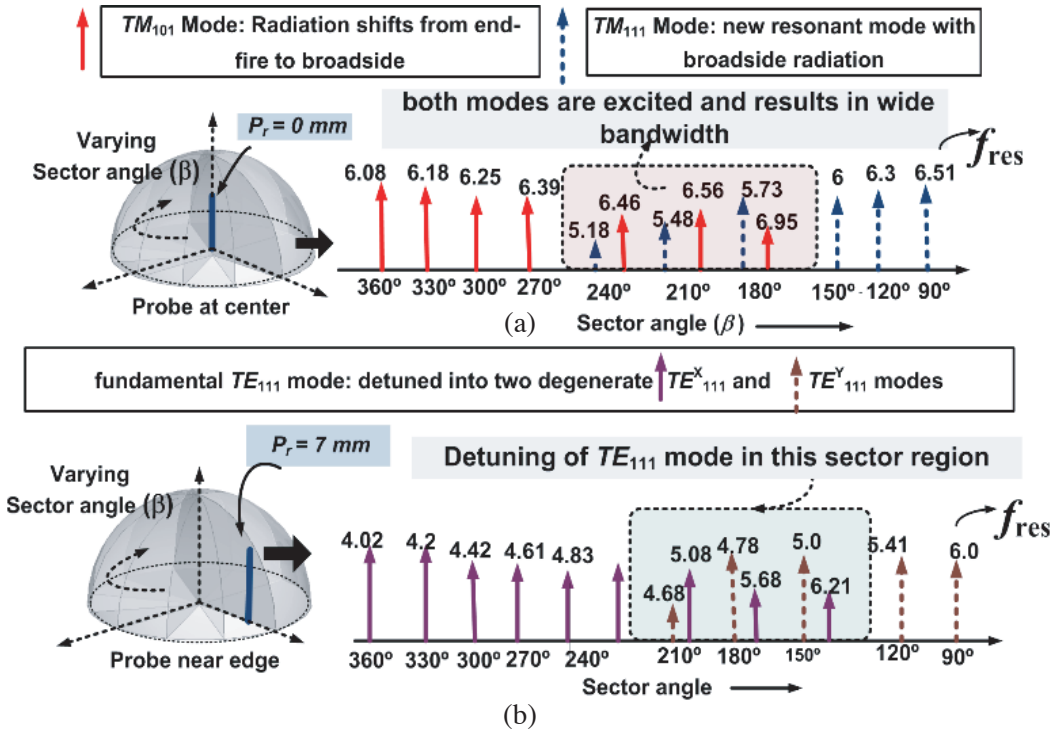


Figure 5. Spectrum of different modes excited in sectorized HDRA (a) $P_r = 0$ mm (b) $P_r = 7$ mm with varying sectorization angle “ β ”. (P_H is chosen at optimized value).

followed by keeping the feed at $P_r = 7$ mm for observing the effect of antenna performance operating at broadside TE_{111} mode. Fig. 5(a) shows the impact of sectorization on different modes excited in sectorized HDRA with their respective resonance frequencies (f_{res}) for $P_r = 0$ mm.

It has been observed that TM_{101} mode is dominant in the range $360^\circ < \beta \leq 270^\circ$, but as ‘ β ’ is further decreased, a new resonant mode appears in close proximity to TM_{101} mode. This mode is identified as TM_{111} mode and radiates like a horizontal magnetic dipole with broadside radiation. TM_{101} mode behaves like a confined mode [13, 14] at $\beta = 360^\circ$, where the boundary condition $\hat{n} \times \vec{H} = 0$ is satisfied, and it radiates like a vertical electric monopole which results in a null in broadside direction. However, by varying β , two inner flat surfaces are formed spaced at different angles such that $\hat{n} \times \vec{H} \neq 0$. Therefore, it becomes partially non-confined type, and the magnetic dipole term becomes more dominant shifting the radiation to broadside. From field distribution view, the fields lying in the xy -plane are out of phase and cancel each other at $\beta = 360^\circ$, but same fields become asymmetric with respect to each other when β is varied due to which full radiation cancellation does not occur, and at $\beta = 180^\circ$ degree, maximum radiation is obtained along broadside direction. The second observation is that a new resonant non-confined type TM_{111} mode is excited due to sectorization. This is a new observation, and it is helpful for getting wide bandwidth as the result of mode merging. However, a similar mode was identified with broadside radiation in [7], in which it was called as $HEM_{11\delta}$ -like mode and was considered as a mode similar to the fundamental mode of cylindrical DRA. In this work, this new mode is named as TM_{111} by observing its field distribution. The input reflection coefficient and driven mode field distribution is shown in Fig. 6(a) and Figs. 7(a)–(e) for verification purpose. Thus, by varying the design parameter ‘ β ’ in the structure keeping feed at $P_r = 0$ mm, an extra resonant mode is observed in sectorized HDRA. In the second case, the probe is fed near the edge ($P_r = 7$ mm), and interesting results are observed. Initially, fundamental TE_{111} mode is excited, but as ‘ β ’ decreases, a second resonant mode appears in close proximity to TE_{111} mode from $210^\circ \leq \beta$. This mode has been identified as a degenerate counterpart of TE_{111} mode. In conventional HDRA, TE_{111}^x and TE_{111}^y modes have the same resonant frequency and propagation constant. However, due to changing the variable parameter β , the geometry of HDRA becomes irregular along azimuthal direction due to which the

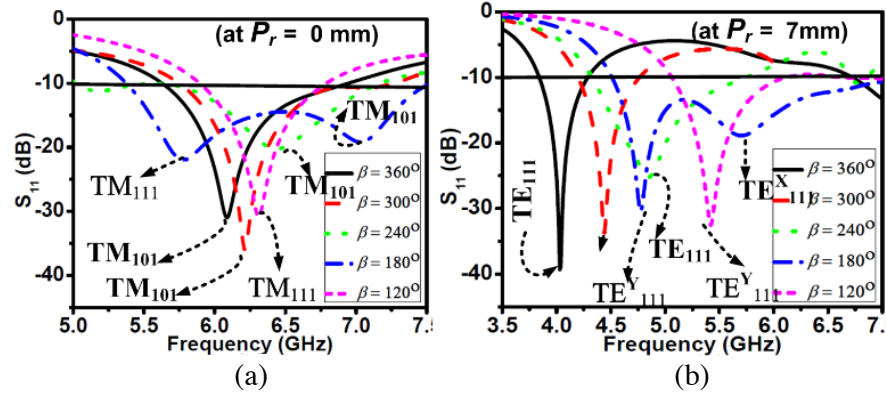


Figure 6. Simulated $|S_{11}|$ in sectorized HDRA at (a) $P_r = 0$ mm (b) $P_r = 7$ mm with varying sector angle “ β ” (only some β values are considered for clear picture).

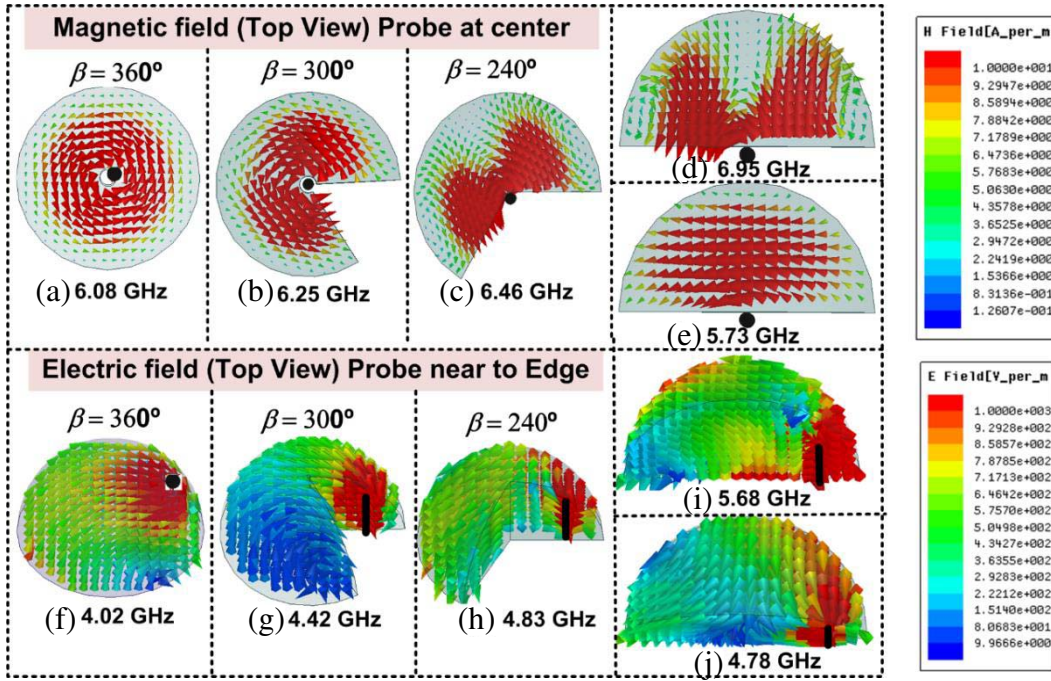


Figure 7. Driven mode magnetic and electric field distribution in sectorized HDRAs (a)–(e) H -field for probe feed at center (f)–(j) E -Field for probe feed near to edge.

time averaged energy stored energy in the electric field and magnetic field gets disturbed. Therefore, the stored energy (which corresponds to quality factor of modes) becomes different, and as a result, the resonant frequency is slightly separated. Thus, TE_{111} mode has been detuned into its orthogonal degenerate counterparts which are identified as TE_{111}^x and TE_{111}^y modes. When β is varied, according to perturbation theory [15], it slightly separates the resonance frequency of the two modes, and this change in resonant frequency is approximated by the change in their electric and magnetic field energies confined in the removed volume.

As the sectorization affects the energy contained in φ -directed fields, the two resonances have unequal energy resulting in the separation in frequency domain. Fig. 6(b) and Figs. 7(f)–(j) show $|S_{11}|$ and driven mode field distribution respectively for the second case. So, it has been observed that by using sectorization technique, extra resonant peaks are excited in particular sector regions, and thus a

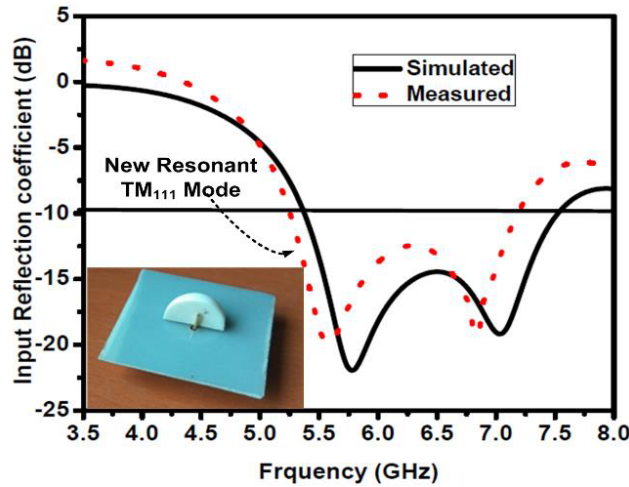


Figure 8. Simulated input reflection coefficient for $\beta = 180^\circ$ when probe feed is located at center position.

possibility of wide bandwidth and circular polarization develops in the structure depending upon feed position. In order to experimentally verify the existence of new TM_{111} mode, an antenna prototype is also fabricated with $\beta = 180^\circ$ and feed position at $P_r = 0$ mm. The corresponding measured and simulated input reflection coefficients are displayed in Fig. 8. Fig. 9(a) shows fractional impedance bandwidth versus “ β ” for different sector geometries for two cases, where wide bandwidth is achieved because of mode merging (as a result of excitation of new mode) at particular sector regions. For the feed at center, wide bandwidth is obtained in the range of $240^\circ \leq \beta \leq 180^\circ$. Thereafter, TM_{111} mode becomes more dominant, and TM_{101} mode disappears reducing the bandwidth also. For the second case, mode merging occurs in $210^\circ \leq \beta \leq 150^\circ$. From observation, the highest bandwidth of 43.7% (4.49 GHz–7.01 GHz) is obtained at $(\beta, P_r) = (180^\circ, 7$ mm), and it is noticed that the bandwidth initially increases and attains the maximum value at $\beta = 180^\circ$, then it decreases. Thus, by varying β , the bandwidth of HDRA at $P_r = 0$ mm is dependent on this parameter. By a proper selection of β , new resonant modes can be excited for wideband applications as a result of mode merging. Fig. 9(b) shows the variation of f_{res} as a function of sector angle ‘ β ’ for both TE_{111} and TM_{101} modes. It is observed that as ‘ β ’ decreases (from 360° to 90°), f_{res} increases for both modes which is obvious due to the decrease in volume, but an interesting point noticed is that the rate of change of f_{res} is different

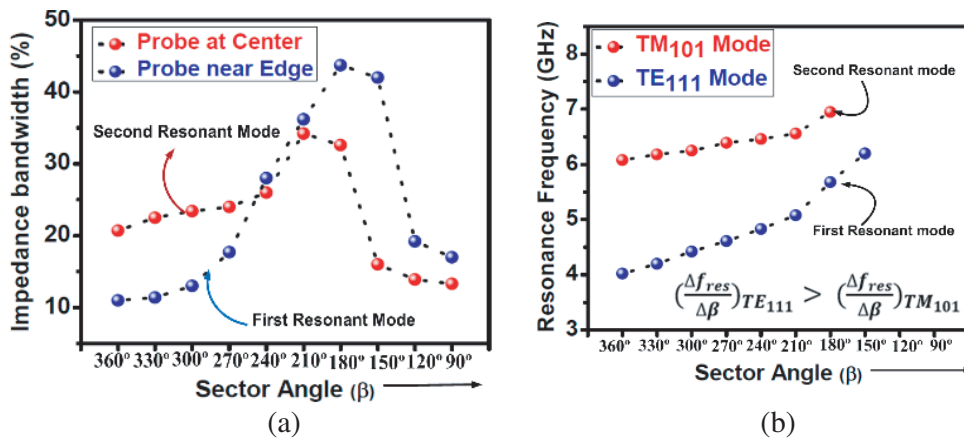


Figure 9. (a) Fractional impedance bandwidth as a function of β for probe at center and edge (b) resonance frequency as a function of ‘ β ’ for TM_{101} and TE_{111} mode.

for the two modes as in Equation (2).

$$\left(\frac{\Delta f_{res}}{\Delta\beta}\right)_{TE_{111}} > \left(\frac{\Delta f_{res}}{\Delta\beta}\right)_{TM_{101}} \quad (2)$$

f_{res} changes rapidly for TE_{111} mode as compared to TM_{101} mode. This is a new observation and can be explained as follows: the resonance frequency (f_{res}) in HDRA is directly proportional to the wavenumber (k_0) inside the HDRA given by Equation (3). [3]

$$f_{res} = \frac{4.7713Re(k_0a)}{a_{cm}} \quad (3)$$

When the design parameter β is changed, the geometry of HDRA becomes irregular along azimuthal direction due to which the time-averaged stored energy in the electric field and magnetic field gets disturbed. Therefore, the stored energy (which corresponds to quality factor of modes) becomes different for different modes. When the same volume of wedge is removed from HDRA, there is more energy loss for TE_{111} mode than TM_{101} mode because for TE_{111} , wavenumber in HDRA is affected by both r - and θ -directed current components whereas for TM_{101} , only r -directed current is affected, and energy lost is less.

Now, sectored HDRAs are investigated for inspecting co-cross polarization characteristics which is an important consideration for the study of polarization purity and CP generation in antenna designs. For the case of conventional HDRA, a huge dependency of co-cross polarization characteristics on probe feed, probe length, and permittivity is reported [16]. Here, we extend a similar investigation to the case of sectored HDRAs which do not appear available in literature. In context of this, ' β ' is varied by keeping feed at two different positions, i.e., $P_r = 0$ mm and $P_r = 7$ mm, and is presented in Figs. 10(a), (b). It is seen that when probe feed is located at the center, E_θ component which is co-fields of TM_{101} mode improves drastically, and radiation is shifted completely from end-fire to broadside by

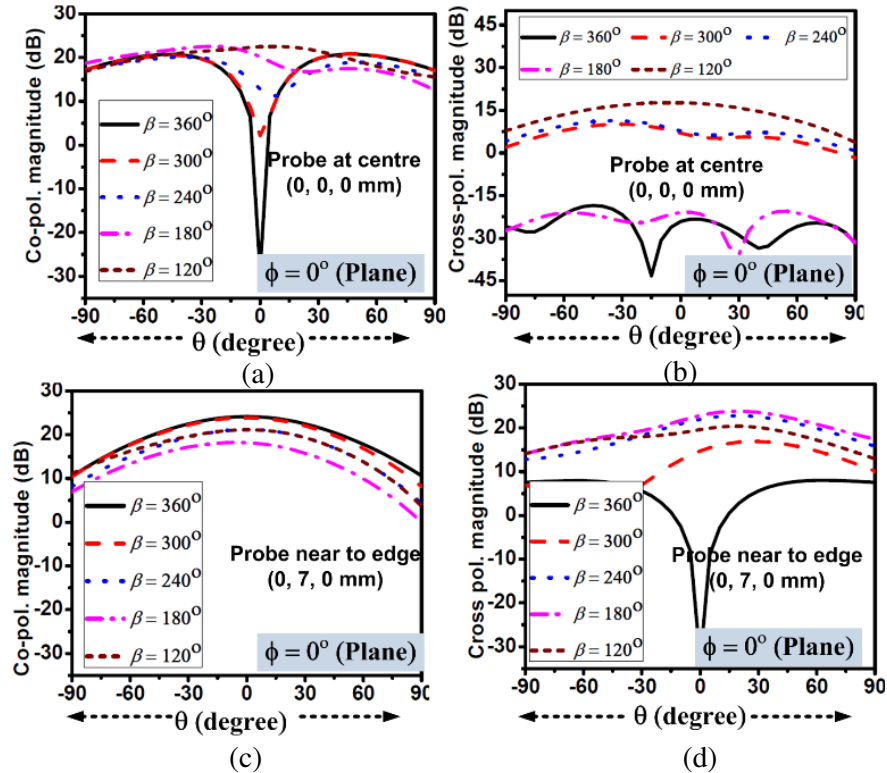


Figure 10. Simulated θ and E_φ component in sectored HDRA at their respective resonance frequencies for (a), (b) probe fed at center (c), (d) probe fed near edge.

changing the value of β from 36° to 18° . This is because, by varying β , the geometry of HDRA becomes irregular, and the field supported by them gets disturbed, due to which the net radiation along broadside direction is cancelled in xz -plane as discussed earlier at $\beta = 180^\circ$. On the other hand, the cross-field of TM_{101} mode, which is φ component, initially increases then decreases at $\beta = 180^\circ$. Considering the polarization purity, feed location should be near the center in sectorized HDRAs as it was not the case with conventional HDRAs. Figs. 10(c)–(d) shows similar results for feed located near the edge where TE_{111} mode is excited. In this case, there is a slight change in the polarization level of φ component, but E_θ component increases considerably after sectorization and remains high thereafter. This performance is not acceptable for the design of a linearly polarized antenna but may be suitable for CP study.

4. CIRCULAR POLARIZATION GENERATION USING SECTROIZATION APPROACH IN HDRA

The procedure for investigating circular polarization requirements in sectorized HDRAs needs a slightly different approach as compared to other sectorized geometries such as sectorized cylindrical DRAs. This is because, unlike CDRAs, in HDRAs, varying the feed position excites both TE and TM modes in the structure, and the identification of orthogonal components becomes difficult.

So, feed position becomes an indispensable parameter which needs to be incorporated in the CP analysis by proper optimization of these two relevant parameters which are sector angle β and feed position (P_r). In this context, these two parameters, ' β ' (varied from 33° to 90°) and " P_r " (varied from 3 to 7 mm), are varied simultaneously, and their CP behavior is checked. Fig. 11 shows the variation of fractional axial ratio bandwidth (ARBW) as feed position for different values of ' β '. The observations made are as follows:

(a) CP obtained in sectorized HDRA is due to two different types of orthogonal modes in different sector regions.

(b) The first one is due to degenerate orthogonal TE_{111}^x and TE_{111}^y modes in sector region $18^\circ \leq \beta \leq 120^\circ$. The maximum ARBW is obtained at $(\beta, P_r) = (180^\circ, 6 \text{ mm})$.

(c) The second one is due to the decomposition of combined modes in which primarily φ -directed and θ -directed E -field components are obtained in sector region $210^\circ \leq \beta \leq 270^\circ$. The maximum ARBW is obtained at $(\beta, P_r) = (270^\circ, 4 \text{ mm})$.

The responsible modes for CP generation along with their resonance frequencies are demonstrated in Fig. 12 for two ' P_r ' values only (for brevity). It has been observed that due to sectorization TE modes are strongly coupled even at $P_r = 4 \text{ mm}$ as it is not the case of conventional HDRA where TE modes are excited with feed near the edge only. This is because θ -directed electric field is strongly coupled, and r -directed field component vanishes due to structure modification. Moreover, combined modes are more significant in the range $360^\circ \leq \beta \leq 210^\circ$ only. Fig. 13 shows field distribution inside sectorized HDRAs where it has been observed that, for fundamental modes, electric fields are decomposed into two orthogonal TE_{111}^x and TE_{111}^y modes (in range of $18^\circ \leq \beta \leq 12^\circ$), whereas electric fields are

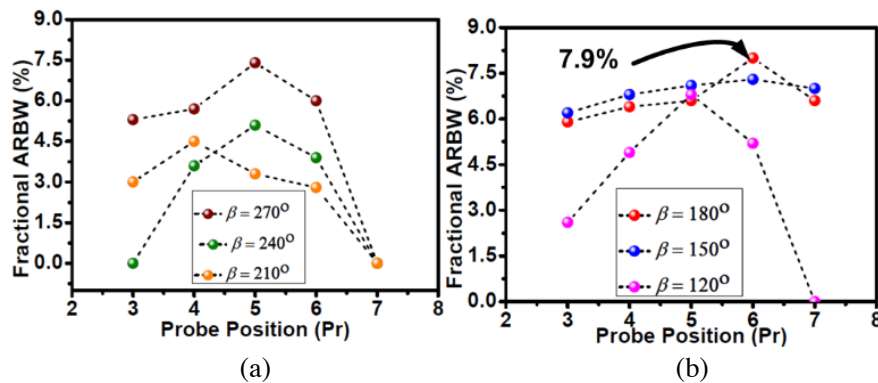


Figure 11. Simulated fractional axial ratio bandwidth (%) for (a) $21^\circ \leq \beta \leq 270^\circ$ and (b) $18^\circ \leq \beta \leq 120^\circ$. (P_H is chosen at an optimized value).

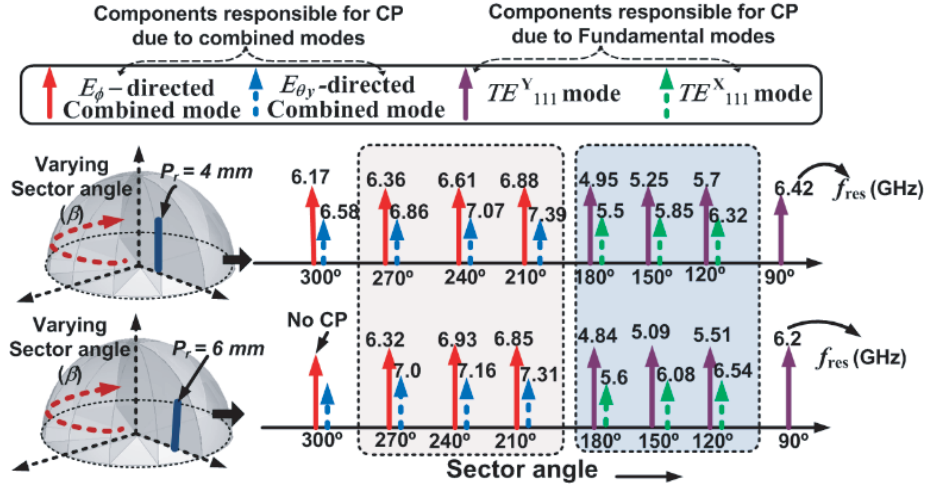


Figure 12. Diagram showing different modes excited in sectored HDRAs considering ‘ β ’ and ‘ P_r ’ simultaneously. (P_H is chosen at an optimized value).

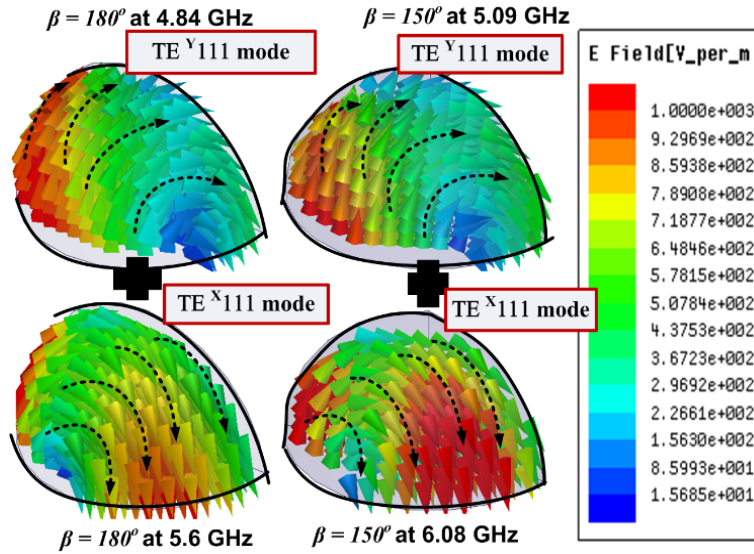


Figure 13. Decomposition of E -fields into orthogonal TE^x_{111} and TE^y_{111} components in sectored HDRA at their respective resonance frequencies with $\beta = 180^\circ$ and 150° (Probe feed at $P_r = 6$ mm).

decomposed into θ -directed and φ -directed components for combined modes ($270^\circ \leq \beta \leq 210^\circ$) as shown in Fig. 14. Thus, orthogonality conditions are visualized inside sectored HDRAs due to sectorization. Additionally, Fig. 15 shows $|S_{11}|$ and AR plot for sectored HDRAs (at $P_r = 4$ mm for combined modes and at $P_r = 6$ for fundamental modes), where two minima in $|S_{11}|$ plot are witnessed which correspond to two orthogonal resonant modes.

4.1. Operating CP Principle for Fundamental Mode

In sectored HDRA, CP is obtained due to detuning of orthogonal degenerate modes of TE_{111} mode by varying β sectorization. At $\beta = 360^\circ$, conventional HDRA excites both TE^x_{111} and TE^y_{111} modes with the same resonant frequency. Sectorization shifts the resonance frequency of orthogonal modes making path length unequal along the azimuthal direction. From electromagnetic simulations, it is revealed that TE^y_{111} is excited at 4.78 GHz, and TE^x_{111} is excited at 5.68 GHz. The ratio of two orthogonal

degenerate modes should be in between 1.01 and 1.10 and may be extended up to 1.2 [17] when individual bandwidth of mode is large. Here the ratio is 1.18, and it satisfies the criteria. When frequency of excitation is properly selected, at a center frequency (f_o) in between these two orthogonal resonances, the amplitudes of both modes will be equal, and phase shift from both will be 4° resulting in phase quadrature relationship between them. Further, optimizing the feed position, maximum ARBW is obtained at $P_r = 6$ mm for this case. There is another observation from Fig. 11 that at fixed feed position

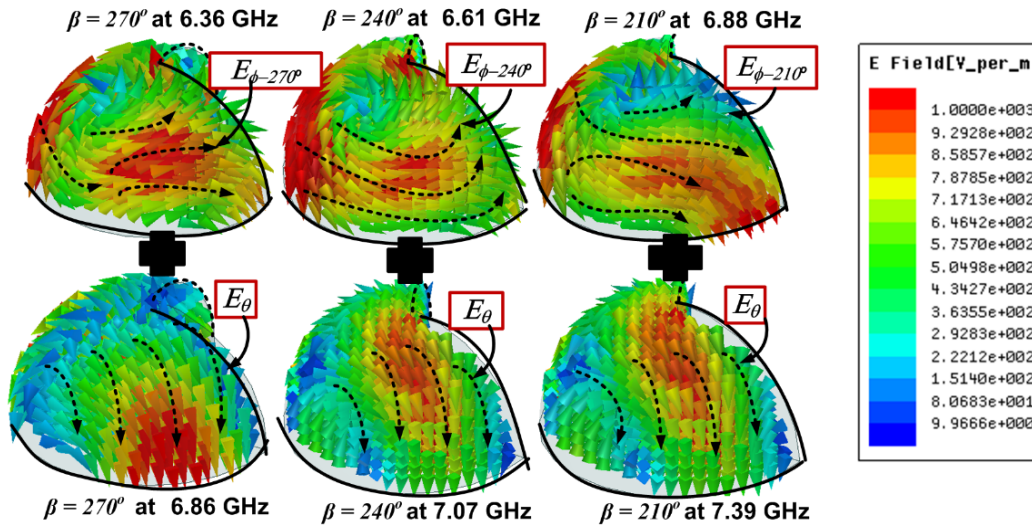


Figure 14. Decomposition of E -fields into orthogonal E_θ and E_ϕ components in sectored HDRA at their respective resonance frequencies with $\beta = 270^\circ$, 240° and 210° (Probe feed at $P_r = 4$ mm).

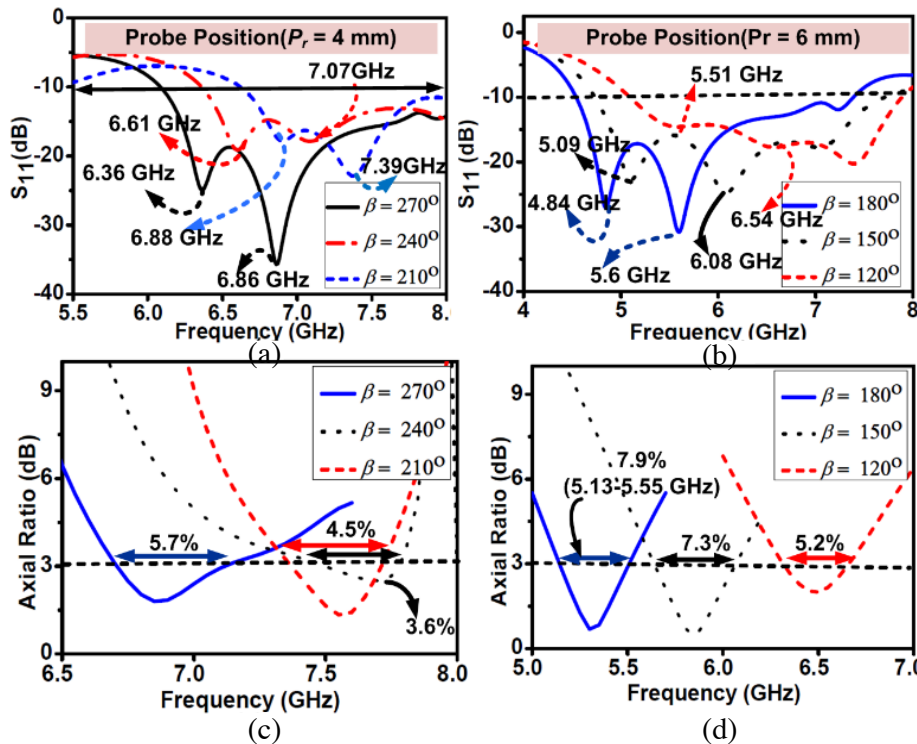


Figure 15. Simulated (a)–(b) Input reflection coefficient and (c)–(d) Axial ratio in sectored HDRA.

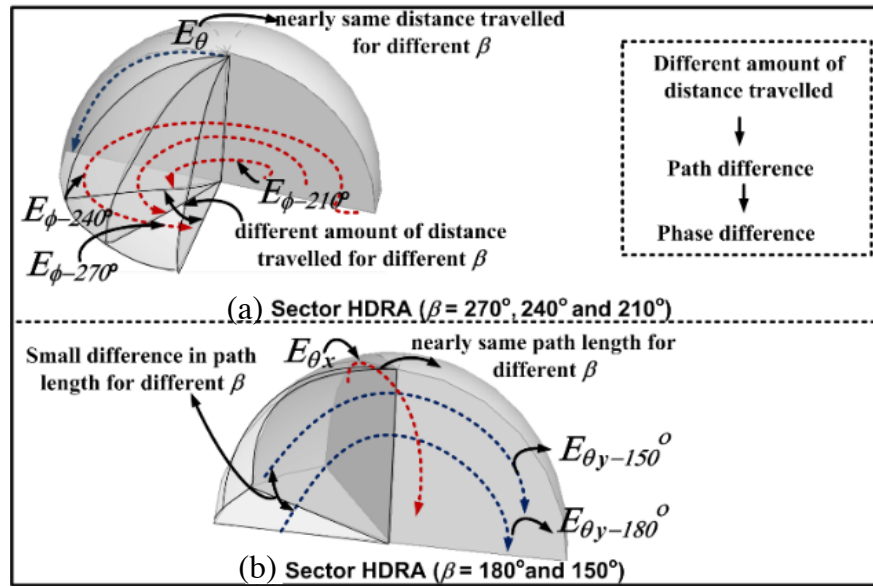


Figure 16. Interpretation of phase difference in sectored HDRAs.

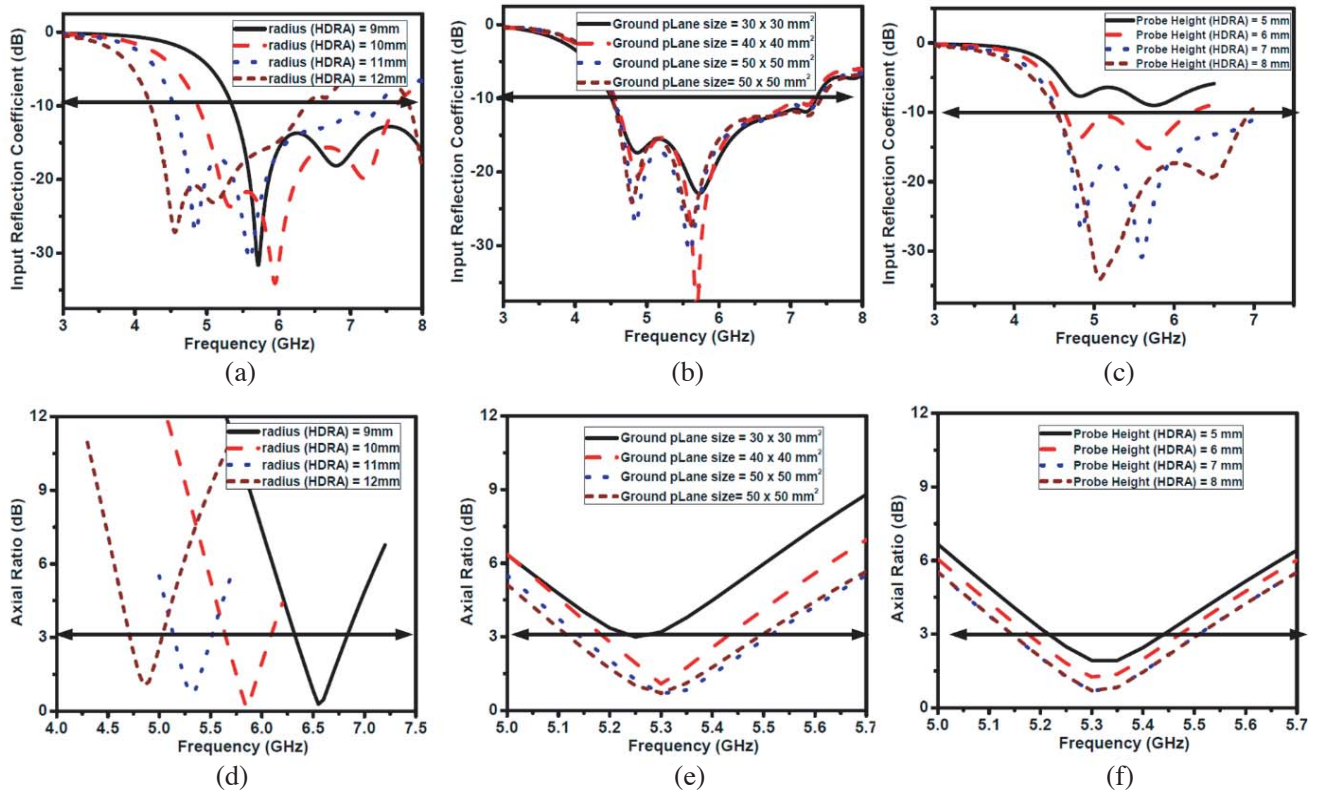


Figure 17. Simulated input reflection coefficient for different value of (a) radius of HDRA (b) Ground plane size (c) Probe height and axial ratio plot for different values of (d) radius of HDRA (e) Ground plane size (f) Probe height. (Parametric analysis has been performed on final proposed antenna).

also, graph shows variation in ARBW for combined modes whereas for fundamental modes variation of ARBW is not significant. This can be explained by the unequal path length between field components in different sectorized DRAs which slightly introduces a change in phase among orthogonal components in the same dielectric medium [18]. In this regard, Fig. 16 demonstrate this phase difference interpretation in sector HDRAs. For conventional HDRA, there is no path difference between φ and E_θ component due to geometrical symmetrically form of HDRA and thus phase difference is not possible. But, when sectorization is introduced, HDRA becomes asymmetric in azimuthal direction and consequently path length for E_φ is altered according to ' β ' values whereas path length for θ almost remains fixed. Now, both E_φ and E_θ components are excited for $\beta = 270^\circ, 24^\circ,$ and $210^\circ,$ and the distance travelled by E_φ component as labeled by φ - $270^\circ, \varphi$ - $240^\circ, \varphi$ - 21° is altered according to β values whereas θ is same for all. This is accountable for path difference and consequently phase difference in the structures as interpreted in Fig. 16(a). Thus, accordingly there is considerable variation in ARBW plot shown in Fig. 11(a). In the case of $\beta = 180^\circ$ and $150^\circ,$ only E_θ directed fields are present which are labeled as $E_{\theta x}$ and $E_{\theta y}$ (correspond to both TE_{111}^x and TE_{111}^y mode) as shown in Fig. 16(b), and thus very minor change in path difference is obtained. Accordingly, there is minor difference in ARBW plot shown in Fig. 11(b). With reference to Fig. 11, the maximum ARBW is obtained at $\beta, P_r = (180^\circ, 6 \text{ mm}).$ Thus $\beta = 180^\circ$ is chosen as the final CP design.

A parametric analysis has been conducted on the radius of HDRA, ground plane size, and probe height to find the optimized design values. The corresponding input reflection coefficient and axial ratio plot are displayed in Fig. 17. Based on the simulation results, an antenna prototype is modelled for finalized CP antenna design with $\beta = 180^\circ$ and $P_r = 6 \text{ mm}$ to validate the simulation results and is demonstrated in Fig. 18.

The measurement result for $|S_{11}|$ is shown in Fig. 19(a), where 47.3% (4.54–7.35 GHz) and 47.4% (4.28–6.94 GHz) of simulated and measured impedance bandwidths are achieved respectively. Simulated radiation efficiency is shown in Fig. 19(a) where good average efficiency of 94% has been achieved. Far field parameters are measured in an anechoic environment for gain and axial ratio ($\varphi = 0^\circ, \theta = 0^\circ$)

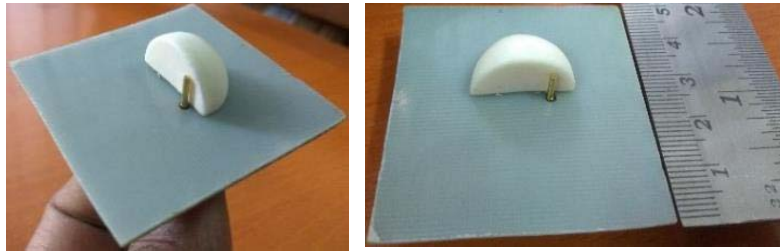


Figure 18. Fabricated prototype of finalized CP design ($\beta = 180^\circ$).

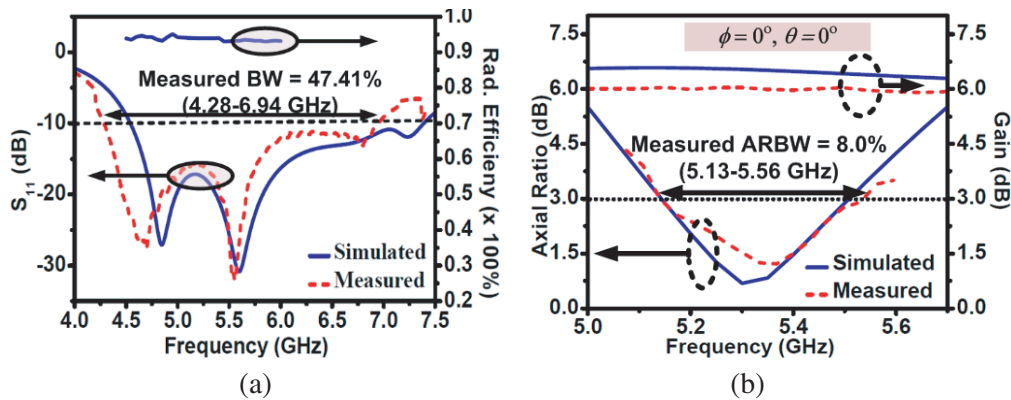


Figure 19. (a) Simulated and measured input reflection coefficient with simulated radiation efficiency (b) simulated and measured axial ratio and gain of proposed antenna ($\beta = 180^\circ$) ($\varphi = 0^\circ, \theta = 0^\circ$).

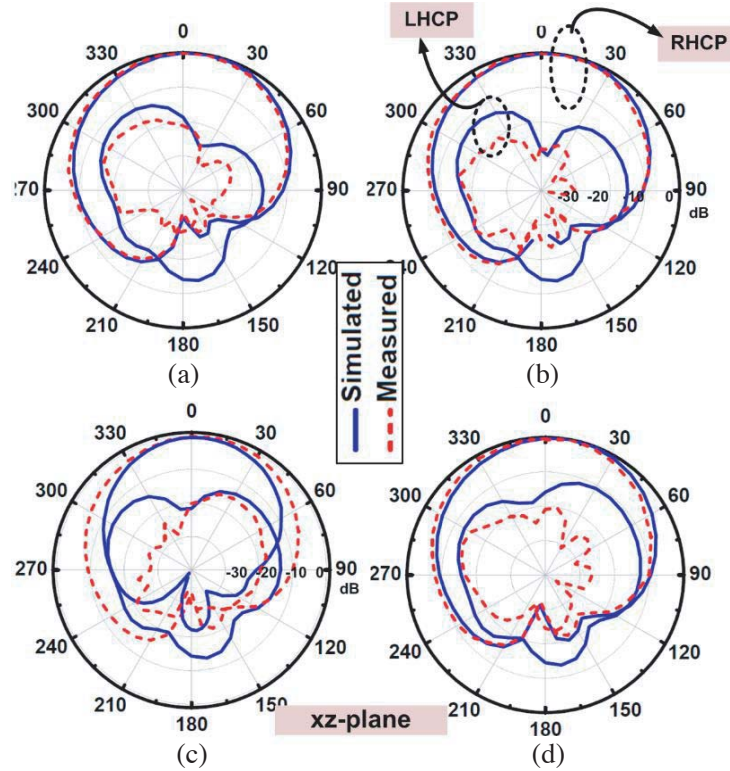


Figure 20. Simulated and measured radiation pattern of final design at (a) 5.2 GHz and (b) 5.3 GHz (c) 5.4 GHz (d) 5.5 GHz.

as shown in single plot in Fig. 19(b). From observation, simulated and measured ARBWs of 7.9% (5.13–5.55 GHz) and 8.0% (5.13–5.56 GHz) are observed with an average gain of 5 dBic in the operating band. Fig. 20 shows radiation patterns at 5.2 GHz, 5.3 GHz, 5.4 GHz, and 5.5 GHz, where right-handed circularly polarized (RHCP) fields are more dominant over left-handed circularly polarized (LHCP) fields by -27 dB and -21 dB, respectively, making this antenna work in RHCP mode.

5. CONCLUSION

Sectorization technique has been applied to HDRAs for the first time. The effect of varying sector angle ' β ' has been analyzed which provides extra resonant modes in HDRA. Further, analysis of CP is conducted on sectorized HDRAs. It has been revealed that the sector angle helps in detuning the degenerate orthogonal modes in HDRA, and thus CP has been obtained by proper optimizing relevant parameters. From complete investigation, a sectorized HDRA with $\beta = 180^\circ$ has been chosen as finalized design among all. Measured results show impedance and AR bandwidth of 47.4% (4.28–6.94 GHz) and 8.0% (5.13–5.56 GHz), respectively. The proposed technique of sectorization provides an extra degree of freedom and flexibility to antenna designers for altering the antenna characteristics which is easy to implement, less complex, and stable as compared to existing concepts in literature. So, this can be considered as a new candidate in DRA family.

REFERENCES

1. Petosa, A., *Dielectric Resonator Antenna Handbook*, Artech House, Norwood, MA, USA, 2007.
2. Mongia, R. K. and P. Bhartia, "Dielectric resonator antennas — A review and general design relations for resonant frequency and bandwidth," *International Journal of Microwave and Millimetre-Wave Computer-Aided Engineering*, Vol. 4, No. 3, 230–247, 1994.

3. Leung, K. W., K. M. Luk, K. Y. A. Lai, and D. Lin, "Theory and experiment of a coaxial probe fed hemispherical dielectric resonator antenna," *IEEE Transactions on Antennas and Propagation*, Vol. 41, No. 10, 1390–1397, 1993.
4. Luk, K. M., K. W. Leung, K. Y. A. Lai, and D. Lin, "Analysis of hemispherical dielectric resonator antenna," *Radio Science*, Vol. 28, No. 6, 1211–1218, 1993.
5. Fang, X. S. and K. W. Leung, "Design of wideband omnidirectional two-layer transparent hemispherical dielectric resonator antenna," *IEEE Transactions on Antennas and Propagation*, Vol. 62, No. 10, 5353–5357, 2014.
6. Mukherjee, B., P. Patel, and J. Mukherjee, "A novel cup-shaped inverted hemispherical dielectric resonator antenna for wideband applications," *IEEE Antennas and Wireless Propagation Letters*, Vol. 12, 1240–1243, 2013.
7. Guha, D. and Y. M. M. Antar, "New half-hemispherical dielectric resonator antenna for broadband monopole-type radiation," *IEEE Transactions on Antennas and Propagation*, Vol. 54, No. 12, 3621–3628, 2006.
8. Guha, D., B. Gupta, C. Kumar, and Y. M. M. Antar, "Segmented hemispherical DRA: New geometry characterized and investigated in multi-element composite forms for wideband antenna applications," *IEEE Transaction on Antennas and Propagation*, Vol. 60, No. 3, 1605–1610, 2012.
9. Leung, K. W. and H. K. Nge, "The slot-coupled hemispherical dielectric resonator antenna with a parasitic patch: Applications to the circularly polarized antenna and wideband antenna," *IEEE Transactions on Antennas and Propagation*, Vol. 53, No. 5, 1762–1769, 2005.
10. Gupta, S., V. Killamsetty, M. Chauhan, and B. Mukherjee, "Compact and circularly polarized hemispherical DRA for C-band applications," *Frequenz Journal of RF-Engineering and Telecommunications, De-gruyter*, Vol. 73, Nos. 7–8, 227–234, 2019.
11. Tam, M. T. K. and R. D. Murch, "Compact circular sector and annular sector dielectric resonator antennas," *IEEE Transactions on Antennas and Propagation*, Vol. 47, No. 5, 837–842, 1999.
12. Chowdhury, R. and R. K. Chaudhary, "Investigation on different forms of circular sectored-dielectric resonator antenna for improvement in circular polarization performance," *IEEE Transactions on Antennas and Propagation*, Vol. 66, No. 10, 5596–5601, 2018.
13. Van Bladel, J., "On the resonances of a dielectric resonator of very high permittivity," *IEEE Transaction on Microwave Theory and Techniques*, Vol. 23, 199–208, 1975.
14. Van Bladel, J., "The excitation of dielectric resonators of very high permittivity," *IEEE Transaction on Microwave Theory and Techniques*, Vol. 23, 208–215, 1975.
15. Pozar, D. M., *Microwave Engineering*, 2nd Edition, Wiley, New York, 1998.
16. Leung, K. W., K. K. Tse, K. M. Luk, and E. K. N. Yung, "Cross-polarization characteristics of a probe-fed hemispherical dielectric resonator antenna," *IEEE Transactions on Antennas and Propagation*, Vol. 47, No. 7, 1228–1230, 1999.
17. Kumar, G. and K. P. Ray, *Broadband Microstrip Antennas*, Artech House, Norwood, MA, USA, 2003.
18. Chowdhury, R. and R. K. Chaudhary, "An approach to generate circular polarization in a modified cylindrical-shaped dielectric resonator antenna using PMC boundary approximation," *IEEE Antennas and Wireless Propagation Letters*, Vol. 17, No. 9, 1727–1731, 2018.